# Conceptual design of hollow electron lenses for beam halo control in the Large Hadron Collider*

G. Stancari,† V. Previtali, and A. Valishev
*Fermi National Accelerator Laboratory, PO Box 500, Batavia, Illinois 60510, USA*

R. Bruce, S. Redaelli, A. Rossi, and B. Salvachua Ferrando
*CERN, CH-1211 Geneva 23, Switzerland*

(Dated: 30 October 2014)

Collimation with hollow electron beams is a technique for halo control in high-power hadron beams. It is based on an electron beam (possibly pulsed or modulated in intensity) guided by strong axial magnetic fields which overlaps with the circulating beam in a short section of the ring. The concept was tested experimentally at the Fermilab Tevatron collider using a hollow electron gun installed in one of the Tevatron electron lenses. Within the US LHC Accelerator Research Program (LARP) and the European FP7 HiLumi LHC Design Study, we are proposing a conceptual design for applying this technique to the Large Hadron Collider at CERN. A prototype hollow electron gun for the LHC was built and tested. The expected performance of the hollow electron beam collimator was based on Tevatron experiments and on numerical tracking simulations. Halo removal rates and enhancements of halo diffusivity were estimated as a function of beam and lattice parameters. Proton beam core lifetimes and emittance growth rates were checked to ensure that undesired effects were suppressed. Hardware specifications were based on the Tevatron devices and on preliminary engineering integration studies in the LHC machine. Required resources and a possible timeline were also outlined, together with a brief discussion of alternative halo-removal schemes and of other possible uses of electron lenses to improve the performance of the LHC.



* Fermilab is operated by Fermi Research Alliance, LLC under Contract No. DE-AC02-07CH11359 with the United States Department of Energy. This work was partially supported by the US DOE LHC Accelerator Research Program (LARP) and by the European FP7 HiLumi LHC Design Study, Grant Agreement 284404.

† Email: ⟨stancari@fnal.gov⟩.

**CONTENTS**

I. Introduction 3

II. Motivation and strategy 3

III. Expected performance and parameter definitions 4
A. Electron lenses and collimation with hollow electron beams 4
B. Effects on halo dynamics 6
1. Beam optics and geometrical parameters 6
2. Halo removal rates 6
3. Diffusion enhancement 8
4. Other effects of halo depletion 8
C. Undesired effects on the core 9
1. Current-density asymmetries in the electron beam 9
2. Impedance of the electron beam 10
D. Further experimental tests 10

IV. Hardware specifications and integration studies 10
A. Physical and mechanical features 11
B. Hollow electron guns 11
C. Vacuum 11
D. Electrical systems 12
E. Cryogenics 12
F. Diagnostics and controls 12
G. Impedance of the electron-lens hardware 13

V. Resources and schedule 13

VI. Alternative halo-removal schemes 13

VII. Conclusions 14

Acknowledgments 14

Tables 16

Figures 17

References 23

## I. INTRODUCTION

Hollow electron beam collimation is a novel technique for beam collimation and halo scraping [1, 2]. It was tested experimentally at the Fermilab Tevatron collider [3–6]. A magnetically confined, possibly pulsed, low-energy (a few keV) electron beam with a hollow current-density profile overlaps with the circulating beam over a length of a few meters. If the electron distribution is axially symmetric, the beam core is unperturbed, whereas the halo experiences smooth and tunable nonlinear transverse kicks. The electron beam is generated by a hollow cathode and transported by strong solenoidal fields. The size, position, intensity, and time structure of the electron beam can be controlled over a wide range of parameters.

The technique relies on robust conventional collimators to absorb particles. However, it has several features that can complement a classic multi-stage collimation system. In the case of high-power proton beams, for instance, scraping is smooth, controllable, and the issues of material damage are mitigated. A depletion zone is generated between the proton beam core and the collimator edges, making local energy deposition less sensitive to beam jitter, collimator movements, orbit and tune adjustments, or fast failures in the case of crab-cavity operation. It might be possible to reduce the electromagnetic impedance of the conventional collimator jaws by retracting them with respect to the standard configuration. Enhanced halo diffusion and larger impact parameters may also improve the overall cleaning efficiency; in the case of ions, these effects would reduce uncontrolled losses due to fragmentation.

This method may provide a unique option to complement the LHC collimation system. To study its implementation, a conceptual design for the LHC upgrade was developed within the US LHC Accelerator Research Program (LARP) and the European FP7 HiLumi LHC Design Study. This may then develop into a technical design in 2014, with the goal to build the devices in 2015–2017, after resuming LHC operations and re-assessing needs and requirements with 6.5-TeV protons. Installation during the next long LHC shutdown (LS2), currently scheduled for 2018, would be technically possible. In case of a resource-limited timeline, installation during the following long shutdown (in 2022) is also an option. In this case, more advanced solutions may be tested and included in the design.

## II. MOTIVATION AND STRATEGY

The requirements for improved beam collimation are being addressed with high priority in preparation for the energy and high-luminosity upgrades of the LHC. The present estimates are based on the operational experience accumulated at 3.5 TeV and 4 TeV during the LHC Run 1 and indicate that the halo cleaning performance of the present collimation system is expected to be adequate for operations after the current long shutdown (LS1) [7, 8]. Caveats obviously apply due to the uncertainty on the extrapolations to higher beam energies, intensities and luminosities. A recent review of the LHC collimation project strongly advised to study possible improvements of the present system [8]. While final decisions on further upgrades can only be taken after sufficient operational experience at higher energy, it is important to continue critical

studies to identify possible improvements for implementation in the next long shutdown (LS2), starting in 2018. Hollow electron beam collimation is considered as a promising option to enhance the present LHC collimation.

In 2012, the primary collimator settings cut into the beam halo down to $4.3\sigma_p$ (where $\sigma_p$ is the rms proton beam size calculated for a beam emittance of 3.5 $\mu$m), which was required to push the amplitude function at the collision points $\beta^*$ down to 60 cm [9]. This corresponded to half gaps of about 1 mm, i.e. as small as the nominal design values for 7-TeV operations. Under these conditions, and contrary to what was observed in previous years with more relaxed collimator settings, the operation was significantly affected by beam losses throughout the operational cycle [10]. About 40 fills were lost due to various beam instabilities before establishing collisions. The interplay between collimator impedance and beam-beam effects is being investigated as a possible source of beam losses. The outcome of a dedicated hollow electron lens review [11] indicated that the functionality of the hollow electron beams demonstrated at the Tevatron would be very useful to improve the LHC operation is case of the beam losses observed in 2012.

The present collimation system cannot easily be used for active and smooth halo scraping during high-intensity operations. Scraping would only be possible by intercepting halo particles with primary collimator jaws, resulting in sharp loss spikes. The operation with bulk material very close to the beam core poses also issues in terms of collimator impedance and material robustness in case of failures, which would not apply if electron beams were used.

It was therefore decided that hollow electron beam collimation studies should be pursued with high priority [12]. The immediate goal is to achieve a technical design report for the construction of 2 hollow electron beam devices by 2015, when the needs for beam scraping at the LHC can be addressed based on solid operational experience at higher energy.

Although they are not the focus of this report, there are other possible uses of electron lenses in the LHC: (a) generation of tune spread for Landau damping to stabilize the beams before collisions; (b) compensation of long-range beam-beam interactions in upgrade scenarios with smaller crossing angles to improve luminosity, as an alternative to compensation wires [13].

## III. EXPECTED PERFORMANCE AND PARAMETER DEFINITIONS

In this Section, we describe the principles of hollow electron beam collimation, its impact on beam halo dynamics, and the causes and mitigation of possible unwanted effects on the beam core. A set of working parameters (summarized in Table I) is derived.

### A. Electron lenses and collimation with hollow electron beams

Hollow electron beam collimation is based on the technology of electron cooling and electron lenses. Electron lenses were developed for beam-beam compensation in colliders [14–16], enabling the first

observation of long-range beam-beam compensation effects by shifting the betatron tunes of individual bunches [17]. They were used for many years during regular Tevatron collider operations for cleaning uncaptured particles from the abort gap [18]. Thanks to the reliability of the hardware, one of the two Tevatron electron lenses (TEL-2) could be used for experiments on head-on beam-beam compensation in 2009 [19], and for exploring hollow electron beam collimation in 2010–2011 [3–5]. Electron lenses for beam-beam compensation were built for the Relativistic Heavy Ion Collider (RHIC) at Brookhaven National Laboratory and are currently being commissioned [20].

Figure 1 shows the layout of the beams in one of the Tevatron electron lenses. The beam is formed in the electron gun inside a conventional solenoid and guided by strong axial magnetic fields. Inside the superconducting main solenoid, the circulating beam interacts with the electric and magnetic fields generated by the electrons. The electron beam is then extracted and deposited in the collector.

The halo of the circulating beam, i.e. particles with betatron amplitudes that exceed the inner radius of the hollow electron beam, is affected by nonlinear transverse kicks (Figure 3). The angular kick $\theta$ experienced by a proton at radius $r$ traversing a hollow electron beam enclosing current $I_{er}$ in an interaction region of length $L$ is given by the following expression:

$$\theta = \frac{2I_{er}L(1 \pm \beta_e\beta_p)}{r\beta_e\beta_p c^2 (B\rho)_p} \left(\frac{1}{4\pi\varepsilon_0}\right), \tag{1}$$

where $v_e = \beta_e c$ is the electron velocity, $v_p = \beta_p c$ the proton velocity, and $(B\rho)_p$ is the magnetic rigidity of the proton beam. The '+' sign applies when the magnetic force is directed like the electrostatic attraction ($\mathbf{v}_e \cdot \mathbf{v}_p < 0$), whereas the '−' sign applies when $\mathbf{v}_e \cdot \mathbf{v}_p > 0$. For example, in a configuration with $I_{er} = 5$ A, $L = 3$ m, $\beta_e = 0.195$ (10-keV electrons), $r = 2.5$ mm, the corresponding kick is $\theta = 0.3$ $\mu$rad for 7-TeV protons. Because of the betatron oscillations of the protons, the transverse kicks have different magnitudes at each turn. The strength of the kicks is proportional to the electron beam current and can be easily controlled. The particles in the core of the circulating beam (whose amplitudes are smaller than the inner electron-beam radius) are unaffected if the distribution of the electron charge is axially symmetric.

The main advantages over conventional collimators are that the transverse kicks are controllable, there is no material deformation or damage, the magnetized hollow electron beam has a low impedance, and the position and size of the electron beam are set by configuring the magnetic-field transport.

The Tevatron experiments on hollow electron beam collimation were conducted on antiprotons, mainly at the end of regular collider stores. In some cases, the electron beam was turned on for the whole duration of the fill after collisions were established. Because of the flexible pulsing pattern of the high-voltage modulator [21], the electron beam could be synchronized with a subset of bunches, providing a direct comparison with the unaffected beam. The main results of hollow electron beam collimation in the Tevatron can be summarized as follows [3–6]:

- the use of the electron lens was compatible with collider operations during physics data taking;
- the alignment of the electron beam with the circulating beam was accurate and reproducible;

- the halo removal rates were controllable, smooth, and detectable;
- with aligned beams and inner electron beam radii above $5\sigma$, there were no intensity or luminosity lifetime changes, or emittance growth in the core; below about $4.5\sigma$, scraping started to occur, with observable effects on luminosity lifetime, but still no measurable core emittance growth;
- loss spikes due to beam jitter and tune adjustments were suppressed;
- the local effect of the electron beam on beam halo fluxes and diffusivities were directly measured with collimator scans.

In this report, we focus on the issues arising from the extension of the technique to the Large Hadron Collider.

### B. Effects on halo dynamics

#### 1. *Beam optics and geometrical parameters*

The LHC primary collimators will be placed at around $6\sigma_p$ from the beam axis. For scraping the halo of a 7-TeV proton beam, we envision the inner radius of the electron beam in the interaction region $r_{mi}$ to be placed between about $4\sigma_p$ and $8\sigma_p$ of the LHC proton rms beam size $\sigma_p = 0.32$ mm. This size is derived from the nominal normalized rms emittance $\varepsilon_p = 3.75$ $\mu$m and the typical amplitude function at the candidate locations, $\beta = 200$ m. Scraping of elliptical proton beams is possible with orbit bumps or by displacing the electron beam, but for simplicity we focus on round beams.

For stability and for transport efficiency, the field in the guiding solenoids should be as large as possible. Based upon previous experience and technical feasibility, we consider configurations where the gun, main (superconducting), and collector solenoids have fields in the ranges $0.2\ \text{T} \le B_g \le 0.4$ T, $2\ \text{T} \le B_m \le 6$ T, and $0.2\ \text{T} \le B_c \le 0.4$ T, respectively. This implies magnetic compression factors $k \equiv \sqrt{B_m/B_g}$ in the range $2.2 \le k \le 5.5$, which sets the required sizes of the cathode inner and outer radii (Figure 4). The 1-inch electron gun cathode built for this purpose (Section IV B), for instance, has inner radius $r_{gi} = 6.75$ mm and outer radius $r_{go} = 12.7$ mm. After magnetic compression, these radii translate to $1.2\ \text{mm} = 3.9\sigma_p \le r_{mi} \le 9.5\sigma_p = 3.0$ mm and $2.3\ \text{mm} = 7.3\sigma_p \le r_{mo} \le 18\sigma_p = 5.7$ mm in the interaction region inside the main solenoid, according to the relation $r_{gi}^2 \cdot B_g = r_{mi}^2 \cdot B_m$ for magnetically confined electron beams.

#### 2. *Halo removal rates*

One of the main goals of the design study is to ensure that halo removal rates for 7-TeV protons are detectable, usable, and calculable.

The scraping experiments at the Tevatron with 0.98-TeV antiprotons were done with peak electron beam currents up to 1.2 A. Halo removal times ranged between seconds and minutes, depending upon the radius and intensity of the electron beam. They were observable both with colliding beams and with only antiprotons in the machine.

The transverse kicks generated by the hollow electron beam are nonlinear and have a small random component due to noise in the electron beam current. These kicks interact with the lattice nonlinearities and with the sources of noise in the machine. Therefore, the kicks needed to obtain a given halo removal rate may not scale directly with the magnetic rigidity of the circulating beam.

Tracking simulations in the Tevatron lattice with the LIFETRAC code showed that relatively small electron currents could significantly enhance halo removal [22]. The removal rates are sensitive to the shape of the electron beam and to the distribution of the halo population. It was observed that tracking codes could give rough but conservative estimates of the removal rates. Numerical simulations of the LHC lattice with the SIXTRACK code indicated that, in the absence of beam-beam interactions and of diffusion processes, removal of 7-TeV protons with a 1-A electron beam current would be slow [23, 24]. These simulations were done with a simplified halo distribution (horizontal only, no momentum spread) and without collisions.

More realistic simulations with the LIFETRAC code were performed in the nominal LHC lattice (V6.503), with nominal beam parameters, at 7 TeV, with and without collisions [25]. The machine lattice did not include multipole errors. The hollow lens had the same nominal parameters (1.2-A total current without turn-by-turn modulations, inner radius at $4\sigma_p$) and it was placed at the candidate location in IR4 (see Section IV A). The cleaning rate for a uniform halo placed between $4\sigma_p$ and $6\sigma_p$ (Gaussian in the longitudinal direction) was 2% of the halo population per hour without beam-beam interactions, and 30% per hour with collisions.

The prototype LHC electron gun (Section IV B) had a yield of over 5 A at 10 keV. This yield should be more than sufficient to have a detectable effect on 7-TeV protons. At the yield of 3.6 A, the simulations predict a halo cleaning rate of 40% per hour without collisions and up to 4% per minute with collisions.

Different pulsing schemes were also pursued to extend the capabilities of the technique, by exploiting the flexibility of the modulator pulsing patterns. Most of the Tevatron scraping experiments were done with the same turn-by-turn excitation intensity on the bunches of interest. However, for beam-beam compensation purposes, the high-voltage modulator was designed to handle bunch-by-bunch adjustments, with 10%–90% rise times of 200 ns [21]. Moreover, fast abort-gap cleaning was achieved by turning on the electron beam every 7th turn, in resonance with the betatron oscillations of the uncaptured beam [18].

In the LHC, one could change the electron beam current turn by turn, synchronizing the voltage change with the abort gap, for instance. Train-by-train (900-ns separation) or even batch-by-batch (225 ns) intensity modulations are feasible; this allows one to preserve the halo on a subset of bunches for diagnostics and machine protection. Bunch-by-bunch adjustments every 25 ns or 50 ns would be challenging and are probably unnecessary.

This flexibility opens up the possibility to operate the hollow electron lens in different pulsing modes:

- *continuous* — the same voltage is applied every turn;

- *resonant* — the voltage is changed turn by turn according to a sinusoidal function (possibly including a frequency sweep to cover the tune spread of the halo), or with the same amplitude, but skipping a given number of turns (as in the Tevatron abort-gap cleaning mode);

- *stochastic* — the voltage is turned on or off every turn according to a random function, or a random component is added to a constant voltage amplitude.

These modes of operation were simulated with tracking codes [23–25]. Both the resonant and the stochastic mode gave significant and tunable halo removal rates. While the first was sensitive to the details of the tune distribution (lattice nonlinearities, beam-beam interactions), the stochastic mode was much more robust.

The introduction of stochastic turn-by-turn modulation of the electron beam current significantly ehnances the halo cleaning efficiency, making the electron lens the dominant loss-driving mechanism. The cleaning rates for the cases with and without beam-beam interactions do not differ as much as in the continuous mode. In either case, 50% of halo is removed in 200 s with a yield of 1.2 A, and 80% at 3.6 A. The maximum cleaning rate attained in the stochastic mode was about 100% per minute.

#### 3. *Diffusion enhancement*

Using collimator scans, it was possible to measure the effects of collisions and of the hollow electron lens on halo diffusion in the Tevatron as a function of betatron amplitude [26, 27]. The hollow electron lens could enhance halo diffusivity in action space by two orders of magnitude. Diffusivities in action space with and without collisions were also measured in the LHC [28]. Halo suppression is the main focus of this project and the main consequence of the drift and diffusion enhancement by the electron beam. However, we intend to further investigate other aspects as well, such as the increase in impact depth on the primary collimators and the possible resulting improvement of collimation efficiency.

#### 4. *Other effects of halo depletion*

Particle removal was not the only effect that could be measured in the Tevatron. Thanks to the gated loss monitors (Section III A), other consequences of halo depletion could be observed [4–6]: the suppression of Fourier components of losses related to beam jitter; the removal of the correlations between losses from different bunch trains due to orbit fluctuations; and the suppression of loss spikes induced by collimator setup or by tune adjustments. Because of the much larger beam power in the LHC, the capability to distribute losses in time may prove very useful.

### C. Undesired effects on the core

#### 1. *Current-density asymmetries in the electron beam*

The core of the circulating beam is unaffected if the distribution of the electron charge is axially symmetric. One possible cause of asymmetry is the space-charge evolution of the electron beam. Other sources of asymmetry are the bends that are used to inject and extract the electron beam from the interaction region.

The electron beam was turned on for several hours during some Tevatron collider stores. With aligned beams and continuous operation, no deterioration of the core lifetimes, emittances, or luminosities were observed. Only a limited number of experiments were done in resonant mode (by skipping turns). In these cases, the electron lens caused emittance growth and luminosity degradation. A quantitative analysis of the experiments is under way.

The current-density profiles generated by the hollow electron guns were measured in the Fermilab electron-lens test stand as a function of beam current and axial magnetic field. Space-charge evolution of the electron beam profiles was mitigated by increasing the guiding magnetic fields. Experiments in the test stand, analytical calculations, and numerical simulations with the WARP particle-in-cell code [29] confirmed that, for main fields above 2 T and beam currents up to several amperes, transverse current-density profiles were practically frozen.

The calculation of the electric fields from the measured current density profiles and the generation of the kick maps caused by the bends is described in Refs. [30, 31]. These fields were used as inputs for tracking simulations to estimate beam lifetimes and emittance growth rates. For the Tevatron lattice and working point, the only azimuthal asymmetry seen to cause extra losses in the core was the quadrupole component in a particular resonant mode (pulsing every 6th turn) [22]. In LHC simulations with LIFETRAC, the bends in continuous mode had no effect on lifetimes, emittances, or dynamic aperture [25]. However, the simulations suggest that, for the stochastic mode, the uncompensated dipole component of the bending section kick may introduce emittance growth that depends on the electron lens design. Namely, the gun-side and collector-side bending sections of the electron lens can be either on the same side of the device (as in the Tevatron and RHIC electron lenses), or on opposite sides of the device with respect to the beam propagation. In the former case, the dipole components of horizontal kick from the bends add up, which leads to the horizontal emittance growth. In the latter case, the dipole components subtract leaving only higher order multipole harmonics. The impact of these higher order harmonics on luminosity lifetime is estimated at about 1% per hour. Although this effect is undesirable, it is slow compared to the scraping time scales envisioned for the stochastic mode. Moreover, further optimizations of the bending sections are possible. Because the stochastic mode of operation offers greater flexibility, the above considerations point towards an electron lens design with the gun and the collector bends on opposite sides.

### 2. *Impedance of the electron beam*

An early concern on the use of electron lenses for beam-beam compensation in colliders was the stability of the beams. The electron beam is continuously renewed, so only intrabunch effects were important in the Tevatron. In particular, a displaced head of the circulating bunch could distort the electron beam, whose electromagnetic fields could in turn act back on the bunch tail, causing oscillations in the electron trajectory and a fast transverse mode coupling instability. A 10-keV electron beam traverses the overlap region of 3 m in about 50 ns. For LHC bunch spacings of 25 ns or 50 ns, coupled-bunch modes may need to be included.

The electron beam is made stiff by increasing the axial solenoidal field, reducing its effective impedance. Instability thresholds for the head-on beam-beam case were estimated in Ref. [32]. The stability of the system was indirectly confirmed by routinely operating the Tevatron electron lenses above 1 T. For the hollow-beam case, requirements are expected to be much less stringent because of the smaller fields generated by a distorted hollow density distribution near its axis. The impedance of the electron-lens hardware (without electron beam) is discussed in Section IV G.

## D. Further experimental tests

Electron lenses for head-on beam-beam compensation are being commissioned at RHIC [20]. It was suggested that further experiments with hollow electron beams on protons for the LHC could address some of the operational scenarios not tested at the Tevatron, such as dynamical use during ramp and squeeze, or a systematic study of pulsed modes.

Although appealing, this option does not appear very likely due to the priorities and beam availability at BNL. Obviously, the first priority is to commission the electron lenses for beam-beam compensation. The 2014 run will focus on ion operations with Au-Au collisions. The earliest operation with protons ($p$-$p$ or $p$-Au) is currently scheduled for 2015.

# IV. HARDWARE SPECIFICATIONS AND INTEGRATION STUDIES

In this Section, we describe some of the practical aspects of the implementation of electron lenses in the LHC, taking into account what was achieved with the Tevatron and RHIC electron lenses and the specific LHC conditions. This work will serve as the basis for a detailed technical design report. Table I summarizes the main characteristics of the device. A detailed description of the Tevatron hardware can be found in Ref. [15].

### A. Physical and mechanical features

The second Tevatron electron lens (TEL-2) occupies 5.8 m of tunnel length, is 1.7-m wide, 1.5-m tall (including current and cryogenic leads), and weighs about 2 t. The radius of the cryostat is 0.3 m. We first considered reusing TEL-2 and installing it in the LHC. Candidate locations (RB-44 and RB-46) were identified on each side of the radiofrequency insertion at IR4 (Figures 5 and 6). In addition to the available longitudinal space, these locations were originally chosen because of the availability of cryogenic infrastracture and because of the large interaxis distance (420 mm) between the two beam pipes to accomodate the TEL-2 cryostat. Beam optics is also favorable (Figure 7): the beams are practically round and the lattice functions are of the order of 200 m. Three-dimensional drawings of TEL-2 were produced. Preliminary integration studies by Y. Muttoni's team showed that the hardware would fit, but it would require a rotation of the cryostat and of the gun/collector solenoids (Figure 8). Although this is feasible, the design of new cryostats for the LHC tunnel would probably be preferable.

### B. Hollow electron guns

A prototype hollow electron gun for the LHC was designed, built, and tested at the Fermilab electron-lens test stand (Figure 9). Its design was based on previous electron guns used in the Tevatron. The tungsten dispenser cathode with BaO:CaO:$Al_2O_3$ impregnant has an annular shape and a convex surface to increase perveance [33]. The outer diameter is 25.4 mm and the inner diameter is 13.5 mm. A filament heater was used to reach the operating temperature of 1400 K. The shape of the extraction electrodes to achieve the desired current-density distribution in the space-charge-limited regime were calculated with the ULTRASAM code [34]. This gun had a perveance of 5.3 $\mu$perv. This means that it could yield more than 5 A of peak current at a cathode-anode voltage of 10 kV (Figure 10). The current-density distribution was measured as a function of voltage and of axial magnetic field. The results of the characterization were reported in Refs. [35, 36].

### C. Vacuum

The Tevatron electron lenses were evacuated with 4 ion pumps (255 l/s nominal total) and reached a typical residual pressure of $10^{-9}$ mbar. The insulating vacuum between the cold mass and the warm beam pipe was $10^{-6}$ mbar. Accessible components were baked with heat tapes, whereas baking of inner surfaces was provided by heating foils. In the LHC, the electron lens has to include, on each side, a vacuum isolation module with gate valves, nonevaporable getter (NEG) cartridges, pumps, and vacuum gauges. The length of each of these modules is about 0.8 m. Surfaces need to be certified for pressure and electron-cloud stability (electron-cloud multiplication is suppressed when the solenoids are on).

### D. Electrical systems

The TEL-2 gun and collector resistive solenoids required 340 A to reach 0.4 T. The superconducting main solenoid yielded 6.5 T at 1780 A. The cathode, profiler electrode, anode bias, and collector require 10-kV high-voltage power supplies.

A high-voltage modulator is used to pulse the anode and extract current from the cathode. It needs to deliver 10 kV with a 10%-90% rise time of 200 ns and a repetition rate of 35 kHz (3 times the revolution frequency). This repetition rate would allow synchronization of the electron beam with a subset of bunches for tests and for direct comparison with the unaffected bunches. The modulator requirements for collimation are less stringent than those achieved with the TEL-2 stacked-transformer modulator for bunch-by-bunch voltage adjustments in the Tevatron [21].

### E. Cryogenics

Installation time is dominated by cryogenic integration, which would be similar to that of a stand-alone magnet at 4.5 K. It requires at least 3 months for warm-up, connection of the dedicated supply/return interfaces with the distribution line (QRL), and cool-down. Electron lenses may benefit from the dedicated rf refrigerator proposed for installation in 2018. The Tevatron devices had static heat loads of 12 W for the helium vessel at 4 K and 25 W for the liquid nitrogen shield. Nitrogen is not available in the LHC tunnel, but high-pressure (20 bar) gaseous helium could be used instead for the shield. In the Tevatron, the magnet string cooling system provided a flux of 90 l/s of liquid helium. The quench protection system would have to be integrated with that of the LHC.

### F. Diagnostics and controls

The main superconducting solenoid incorporates 6 corrector magnets (1 long dipole positioned between 2 short dipoles in each plane) for the alignment of the electron beam. Two stripline pickups (each one with both horizontal and vertical plates) are positioned at the upstream and downstream ends of the overlap region for accurate beam position monitoring of both the long electron pulses and the short proton pulses. Sensitive loss monitors (such as scintillator paddles or diamond detectors), positioned at the nearest aperture restrictions, can be used to verify the relative beam alignment. In addition, if the loss monitors are gated and synchronized with subsets of bunches, they can provide a direct comparison between the intensity decay rates, loss fluctuations, and halo diffusivities of bunches with and without the electron-lens effect.

Monitoring of the electron beam profiles can be achieved with flying wires or with fluorescent screens at low currents, and with pinhole scans in the collector at high currents. A direct measurement of the halo population (through synchrotron light or induced fluorescence, for instance), although not strictly necessary, would greatly benefit this project and LHC operations in general [37]. Biased electrodes on each side of the

overlap region can be used for clearing residual-gas ions if necessary.

An electron lens test stand at CERN (possibly in collaboration with the development of the ELENA electron cooler [38]) should be developed to characterize components and to develop diagnostic techniques.

### G. Impedance of the electron-lens hardware

Bunch structure and beam intensities in the LHC are very different from those in the Tevatron. This translates into tighter requirements on the electromagnetic impedance of the electron-lens hardware. (The impedance effects of the electron beam itself are discussed in Section III C 2.) In the Tevatron, the typical rms bunch length was 2 ns and the bunch spacing was 395 ns. In the LHC, the bunch spacing is 25 ns or 50 ns, and the typical bunch length is 0.3 ns.

The total longitudinal impedance of the Tevatron vacuum chamber and components was a few ohms [39], whereas the LHC broad-band longitudinal impedance budget is only 90 mΩ [40]. TEL-2 stretched-wire measurements showed several peaks between 0.1 Ω and 1 Ω in the frequency range 0.1–1 GHz [41], confirming recent preliminary simulations, which identified trapped modes in the electrode structure (injection chamber, clearing electrodes, beam position monitors, etc.) [42]. The design of the electron-lens electrodes will have to include provisions (such as rf shields) to suppress wake fields, but this should not constitute a major obstacle. The preliminary analysis of transverse impedances has not raised any issues so far.

## V. RESOURCES AND SCHEDULE

The construction cost of each of 2 electron lenses (one per beam) for the LHC is estimated to be 2.5 M$ in materials and 3.0 M$ in labor. This includes engineering, electron guns, resistive and superconducting solenoids, vacuum chambers, electrodes, cabling, instrumentation, and controls.

Construction of 2 devices would take about 3 years. Construction in 2015–2017 and installation during a long shutdown in 2018 is technically feasible. Reuse of some of the Tevatron equipment, such as superconducting coils, conventional solenoids, power supplies, and electron guns, is also possible. Fermilab and BNL have the capabilities and facilities for building the electron lens hardware.

Contributions in the areas of design, construction, commissioning, numerical simulations, beam studies, and project management will be specified in an agreement between CERN and US LARP.

## VI. ALTERNATIVE HALO-REMOVAL SCHEMES

Hollow electron beam collimation is being evaluated in comparison with other halo scraping techniques: tune modulation, damper excitation, and beam-beam wire compensators.

Tune modulation with warm quadrupoles was used in HERA at DESY to counteract the effects of power-supply ripple [43, 44]. It was suggested that this technique may allow one to excite a subset of particles in

tune space. Preliminary simulations with the SIXTRACK code indicated that the halo cannot be removed as selectively [24], but further investigations and experimental tests are needed. Narrow-band excitations with the transverse damper system were also proposed as a halo reduction method [45]. Beam tests may be possible in 2015 after resuming LHC operations. Both tune modulation and damper excitation operate in tune space, where the core and the halo of the beam are not necessarily separated.

Wire compensators for long-range beam-beam interactions are another method one could use to manipulate the dynamic aperture in a controlled way. It turns out that magnetically confined pulsed electron beams may actually provide a better alternative not only for scraping but also for long-range compensation, because they are not electrically neutral (therefore requiring much less current), because no material in close proximity with the circulating beam is involved, and because their strength can be different for different bunches [13].

## VII. CONCLUSIONS

Experimental and numerical studies were conducted to support the conceptual design of a hollow electron beam collimator for the LHC, a promising technique for controlled scraping of very intense beams. This technique may be used in all cases in which material damage, localized instantaneous energy deposition, or impedance limit the use of conventional collimators.

The design was based on the experience of the existing Tevatron and RHIC electron lenses. The expected halo cleaning performance and the mitigation of undesired effects on the beam core were inferred from the Tevatron experiments and from numerical tracking simulations. A hollow electron gun with geometrical features and peak current yields appropriate for the LHC was built and tested. To achieve a wide range of halo removal rates, several electron beam pulsing modes were studied. Hardware parameters and instrumentation options were defined. No major obstacles were identified in the integration of the devices in the LHC ring from the point of view of electromagnetic impedance, mechanical engineering, or cryogenics. Required resources were outlined. Studies of possible alternative schemes were initiated. Further experimental tests may be possible with the RHIC electron lenses to extend the Tevatron results. We also identified other uses of electron lenses that could improve the performance of the LHC: generation of tune spread for beam stabilization before collisions; and long-range beam-beam compensation for luminosity upgrade scenarios with small crossing angles.

Our studies suggest that hollow electron beam collimation could be implemented in the LHC, if needed. This conceptual design report will serve as the basis for a detailed technical design.

## ACKNOWLEDGMENTS

This work has greatly benefited from the contributions and support of several people. In particular, the authors would like to thank O. Aberle, A. Bertarelli, F. Bertinelli, E. Bravin, O. Brüning, G. Bregliozzi,

P. Chiggiato, S. Claudet, W. Hofle, R. Jones, Y. Muttoni, L. Rossi, B. Salvant, H. Schmickler, R. Steinhagen, L. Tavian, G. Valentino (CERN), G. Annala, G. Apollinari, M. Chung, T. Johnson, I. Morozov, E. Prebys, G. Saewert, V. Shiltsev, D. Still, L. Vorobiev (Fermilab), R. Assmann (DESY), V. Kamerdzhiev (FZ Jülich), M. Blaskiewicz, W. Fischer, X Gu (BNL), D. Grote (LLNL), H. J. Lee (Pusan National U., Korea), S. Li (Stanford U.), A. Kabantsev (UC San Diego), T. Markiewicz (SLAC), V. Moens (EPFL), and D. Shatilov (BINP).

The authors would like to sincerely acknowledge the CERN colleagues who participated in the 2012 hollow e-lens review (G. Arduini, O. Bruening, S. Claudet, K. Cornelis, J. Coupard, B. Dehning, M. Giovannozzi, B. Goddard, E. Jensen, W .Höfle, A. Grudiev, M. Lamont, R. Losito, R. Schmidt, J. Wenninger, M. Zerlauth) and Steve Myers who chaired the panel that recommended the strategy adopted for the applications for the LHC.

## TABLES

Table I. List of hollow electron lens parameters for the LHC. The requirements on the electron beam current stem from the magnetic rigidity of the proton beam, from the length of the interaction region, and from the size of the electron beam (Section III A). The size of the cathode is determined by the proton beam size, by the desired range of scraping positions, and by the available magnetic fields (Section III B 1).

| Parameter | Value or range |
|---|---|
| *Beam and lattice* | |
| Proton kinetic energy, $T_p$ [TeV] | 7 |
| Proton emittance (rms, normalized), $\varepsilon_p$ [$\mu$m] | 3.75 |
| Amplitude function at electron lens, $\beta_{x,y}$ [m] | 200 |
| Dispersion at electron lens, $D_{x,y}$ [m] | $\leq 1$ |
| Proton beam size at electron lens, $\sigma_p$ [mm] | 0.32 |
| *Geometry* | |
| Length of the interaction region, $L$ [m] | 3 |
| Desired range of scraping positions, $r_{mi}$ [$\sigma_p$] | 4–8 |
| *Magnetic fields* | |
| Gun solenoid (resistive), $B_g$ [T] | 0.2–0.4 |
| Main solenoid (superconducting), $B_m$ [T] | 2–6 |
| Collector solenoid (resistive), $B_c$ [T] | 0.2–0.4 |
| Compression factor, $k \equiv \sqrt{B_m/B_g}$ | 2.2–5.5 |
| *Electron gun* | |
| Inner cathode radius, $r_{gi}$ [mm] | 6.75 |
| Outer cathode radius, $r_{go}$ [mm] | 12.7 |
| Gun perveance, $P$ [$\mu$perv] | 5 |
| Peak yield at 10 kV, $I_e$ [A] | 5 |
| *High-voltage modulator* | |
| Cathode-anode voltage, $V_{ca}$ [kV] | 10 |
| Rise time (10%–90%), $\tau_{\mathrm{mod}}$ [ns] | 200 |
| Repetition rate, $f_{\mathrm{mod}}$ [kHz] | 35 |

## FIGURES

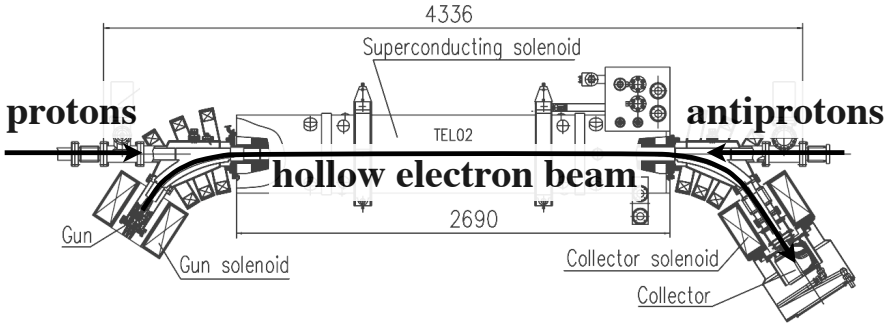


Figure 1. Layout of the beams in the second Tevatron electron lens (TEL-2). The electron beam is generated and accelerated in the electron gun, transported through the overlap region with strong axial fields, and deposited in the collector. Dimensions are in millimeters.

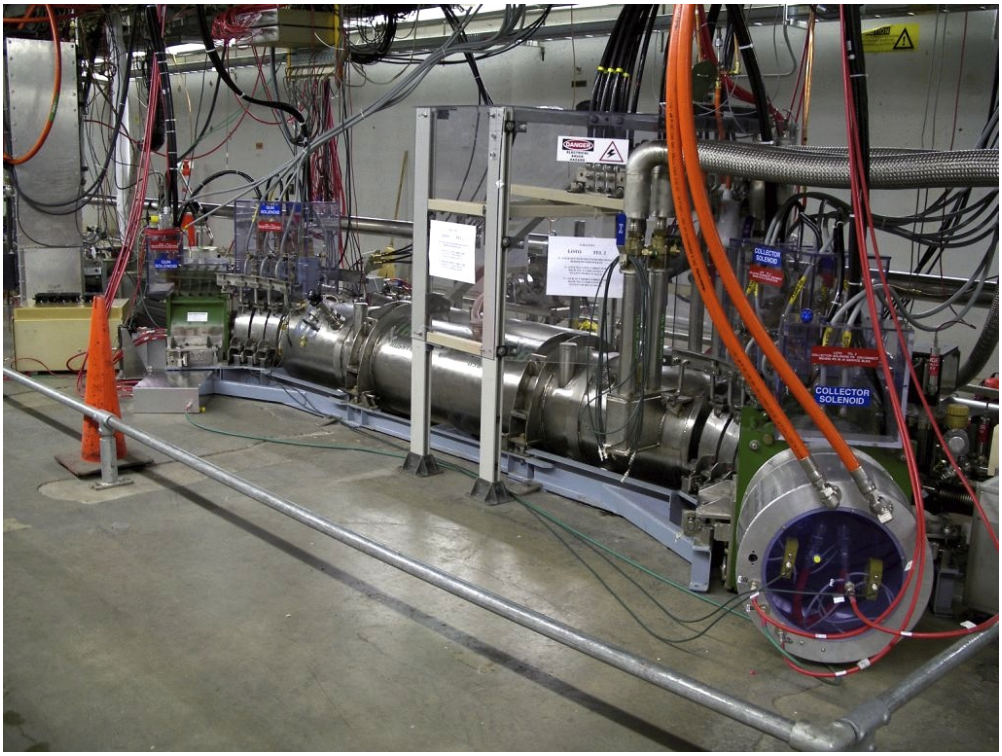


Figure 2. Photograph of the second Tevatron electron lens (TEL-2) after installation in the Tevatron tunnel in 2006.

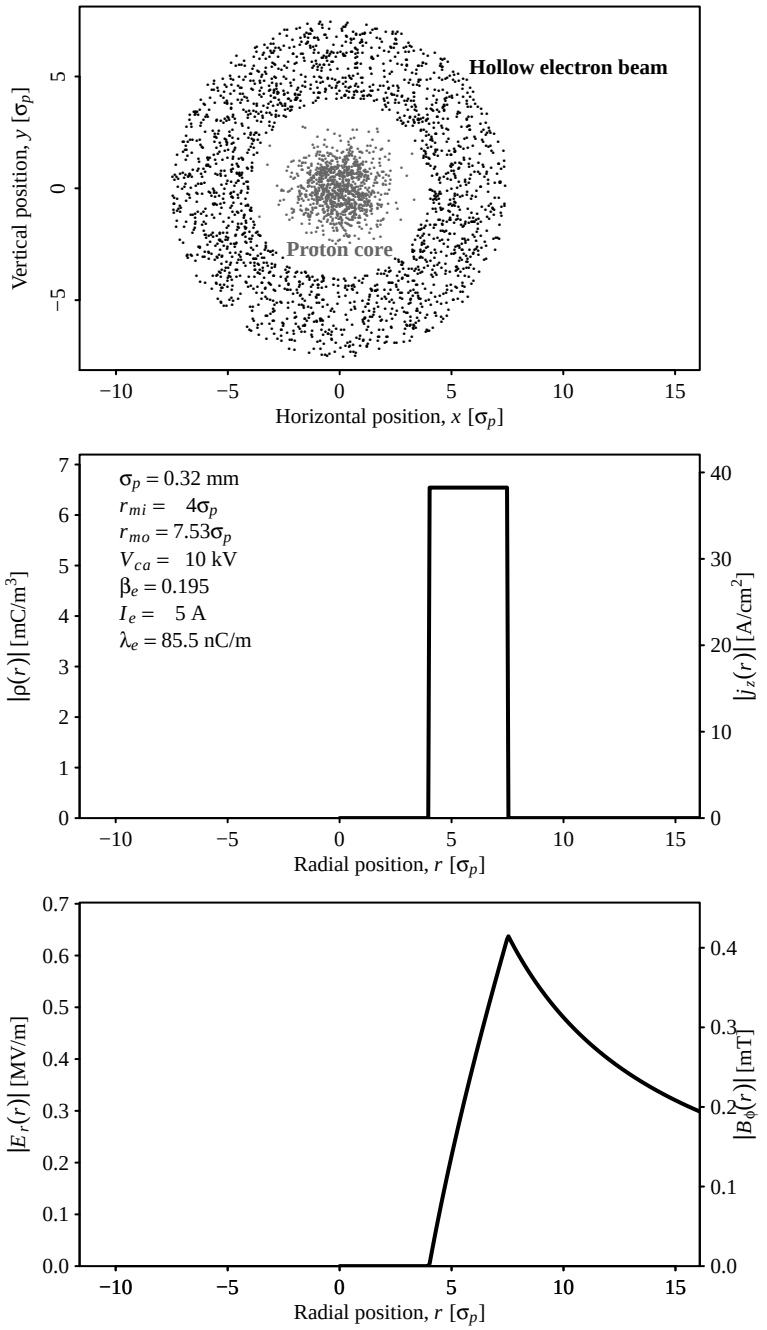


Figure 3. Concept of hollow electron beam collimation. The top plot illustrates schematically the transverse layout of the beams in the overlap region assuming cylindrical symmetry. The bottom two plots show a numerical example: the electron charge density $\rho$ and current density $j_z$ as a function of radial position (middle plot); the radial electric field $E_r(r)$ and azimuthal magnetic field $B_\phi(r)$ generated by the electron beam (bottom plot).

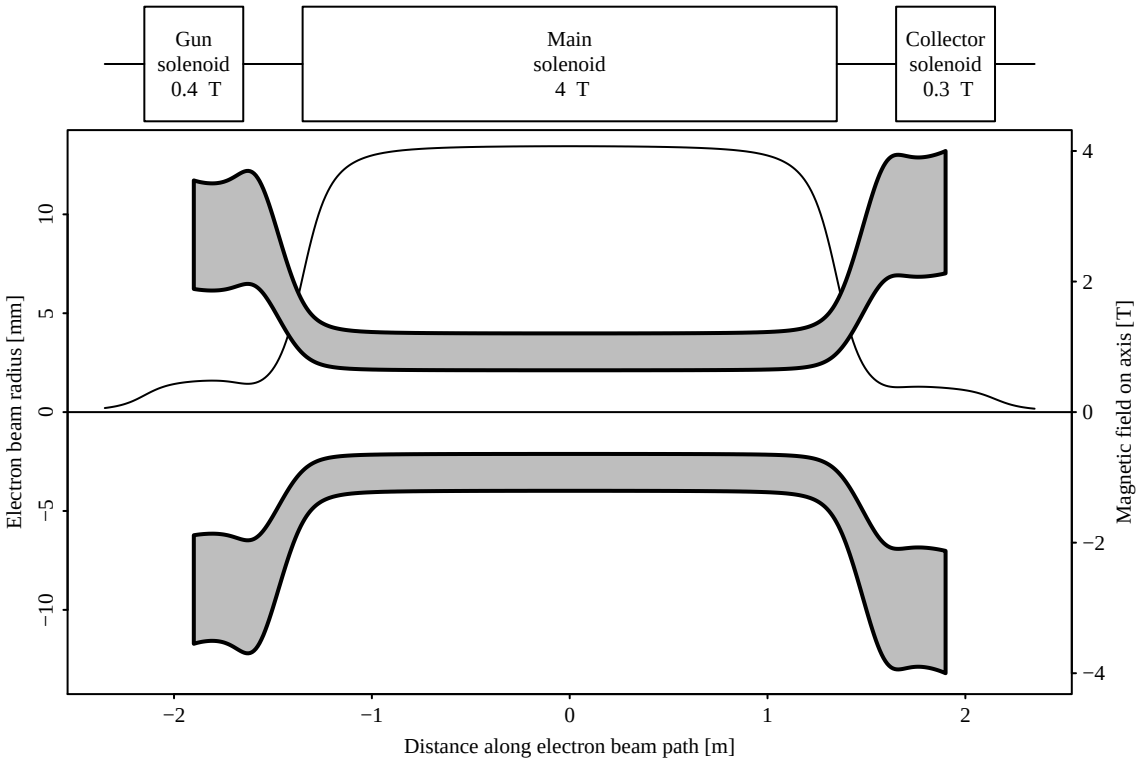


Figure 4. Illustration of magnetic compression of the electron beam (gray) in an electron lens, as the axial magnetic field varies inside the solenoids (thin solid line).

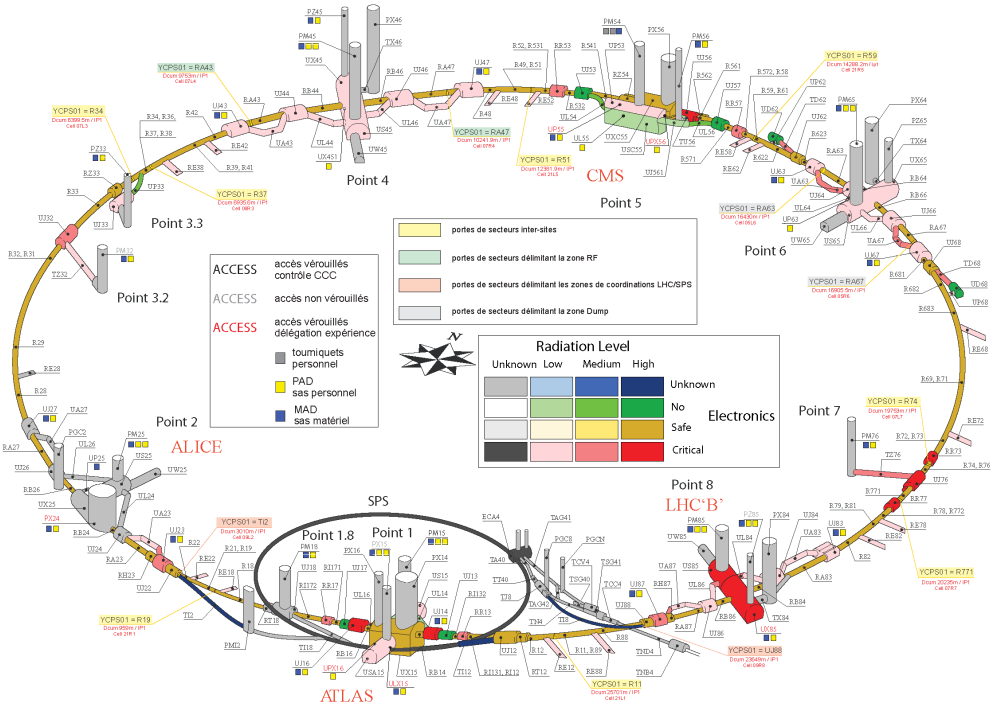


Figure 5. Schematic diagram of the LHC. Candidate locations for the electron lenses are RB-44 and RB-46 at Point 4, on each side of the interaction region IR4, which houses the accelerating cavities.

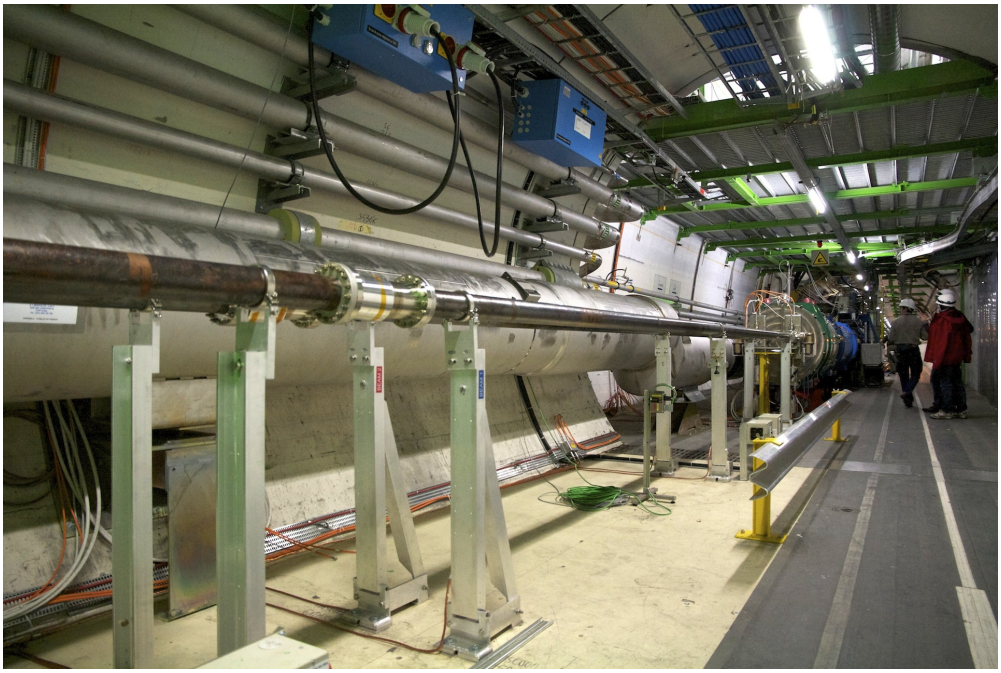

Figure 6. Photograph of RB-46, one of the candidate locations, east of IR4. In this view, Beam 1 is on the inside, moving away from the viewer. The first downstream element is the green synchrotron-light undulator. The interaxis beam-pipe separation is 420 mm. The RB-44 location has a very similar (mirror-imaged) configuration. (Photo taken by V. Previtali on November 10, 2011.)

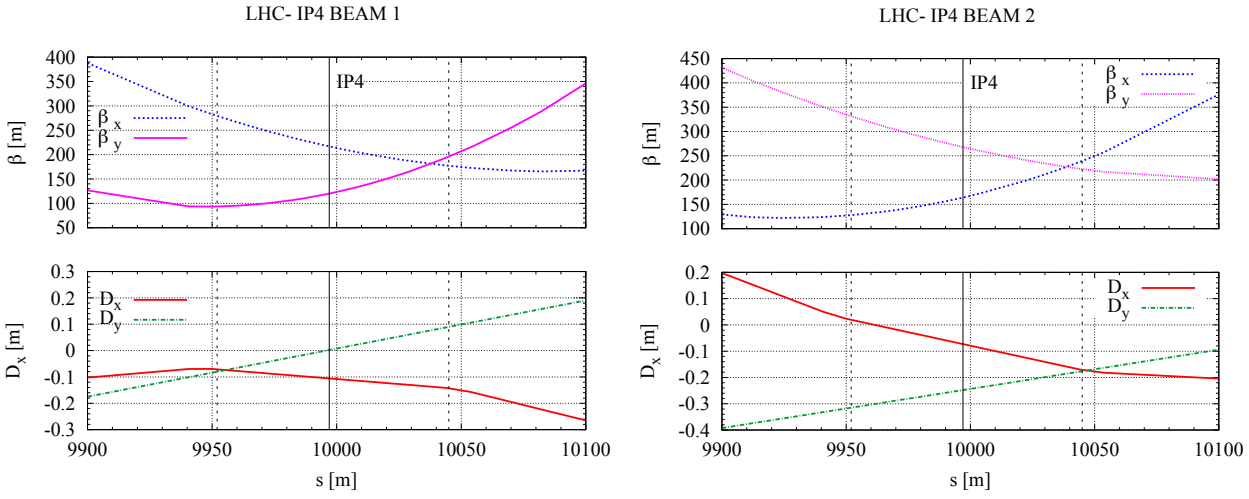


Figure 7. LHC machine lattice near the interaction region IR4. The candidate locations RB-44 (smaller $s$ coordinate) and RB-46 (larger $s$) are marked with the dashed lines.

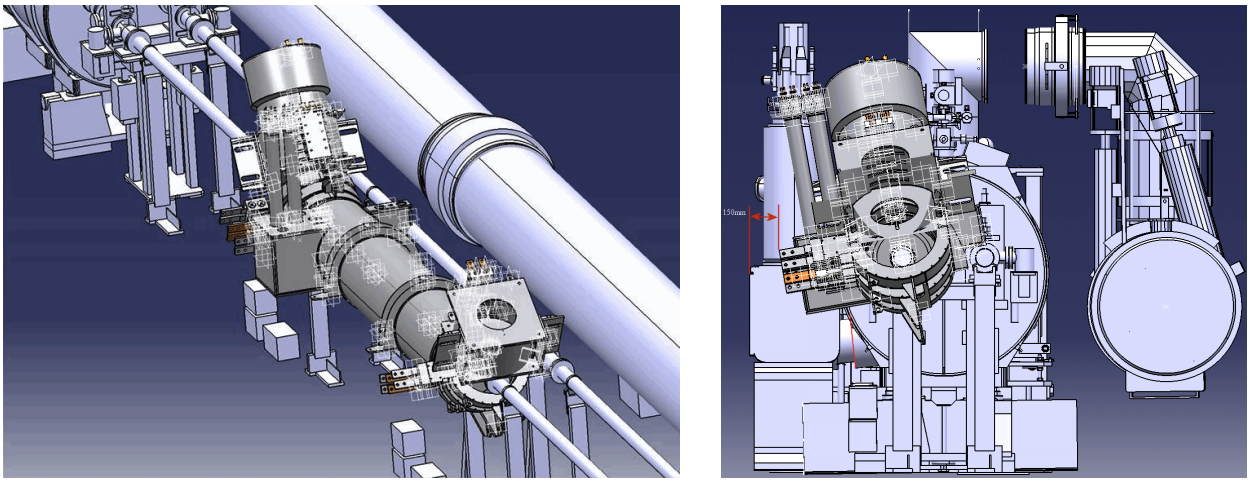


Figure 8. Integration study of a Tevatron electron lens (TEL-2) at the RB-44 location in LHC. Transverse space constraints require a rotation of 80° around the beam axis with respect to the Tevatron configuration.

Figure 9. Assembly of the prototype (1-inch) hollow electron gun. The first photograph shows the base flange with electrical connections. In the second photo, one can see the hollow cathode with convex surface and the rim of the control electrode; both are surrounded by cylindrical heat shields. The mounting of the copper anode is shown in the third picture. The last picture shows the complete assembly.

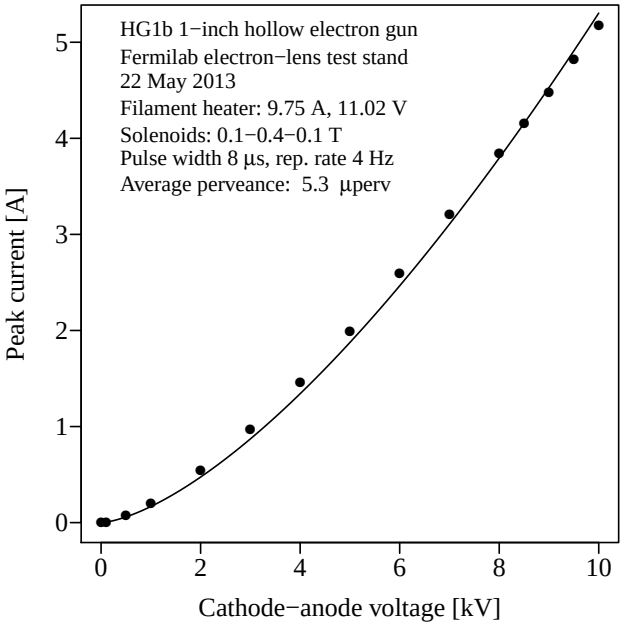


Figure 10. Performance of the prototype (1-inch) hollow electron gun measured at the Fermilab electron-lens test stand. The total peak current at the cathode $I_e$ is plotted as a function of the cathode-anode voltage $V_{ca}$.

[1] V. Shiltsev, in Proceedings of the 3rd CARE-HHH-APD Workshop (LHC-LUMI-06), Valencia, Spain, p. 92, CERN-2007-002 (2007).

[2] V. Shiltsev, in Proceedings of the CARE-HHH-APD Workshop (BEAM07), Geneva, Switzerland, p. 46, CERN-2008-005 (2008).

[3] G. Stancari et al., Phys. Rev. Lett. **107**, 084802 (2011).

[4] G. Stancari, in Proceedings of the Meeting of the Division of Particles and Fields of the American Physical Society, Providence, RI, USA, August 2011, arXiv:1110.0144 [physics.acc-ph], FERMILAB-CONF-11-506-AD-APC.

[5] G. Stancari et al., in Proceedings of the 2011 International Particle Accelerator Conference (IPAC11), San Sebastián, Spain, September 2011, p. 1939, FERMILAB-CONF-11-412-AD-APC.

[6] G. Stancari, 'Beam experience at the Tevatron and status of the hollow electron-lens hardware,' talk presented at the Special Collimation Upgrade Specification Meeting: Internal Review of Tevatron Hollow Electron-Lens Usage at CERN, https://indico.cern.ch/event/213752, Geneva, Switzerland, 9 November 2012.

[7] LHC Collimation Review 2001, http://indico.cern.ch/event/139719, Geneva, Switzerland, 14–15 June 2011.

[8] LHC Collimation Review 2013, http://indico.cern.ch/event/251588, Geneva, Switzerland, 30–31 May 2013.

[9] R. Bruce and R. W. Assmann, 'LHC $\beta^*$reach in 2012,' LHC Beam Operations Workshop 2011, https://indico.cern.ch/event/155520, Evian, France, 12–14 December 2011.

[10] B. Salvachua et al., 'LHC collimation cleaning and operation outlook,' LHC Beam Operations Workshop 2012, https://indico.cern.ch/event/211614, Evian, France, 17–20 December 2012.

[11] Special Collimation Upgrade Specification Meeting: Internal Review of Tevatron Hollow Electron-Lens Usage at CERN, https://indico.cern.ch/event/213752, Geneva, Switzerland, 9 November 2012.

[12] S. Redaelli, 'Overall strategy for electron lenses and action plan for HL LHC,' talk presented at the 2nd Meeting of the Technical Committee for the LHC High-Luminosity Upgrade (HLTC), http://indico.cern.ch/event/236318, Geneva, Switzerland, 8 March 2013.

[13] A. Valishev and G. Stancari, FERMILAB-TM-2571-APC, arXiv:1312.1660 [physics.acc-ph] (2013).

[14] V. Shiltsev et al., Phys. Rev. ST Accel. Beams **2**, 071001 (1999).

[15] V. Shiltsev et al., Phys. Rev. ST Accel. Beams **11**, 103501 (2008).

[16] V. Shiltsev et al., New J. Phys. **10**, 043042 (2008).

[17] V. Shiltsev et al., Phys. Rev. Lett. **99**, 244801 (2007).

[18] X. Zhang et al. Phys. Rev. ST Accel. Beams **11**, 051002 (2008).

[19] G. Stancari and A. Valishev, in Proceedings of the ICFA Workshop on Beam-Beam Effects in Hadron Colliders (BB2013), Geneva, Switzerland, March 2013, FERMILAB-CONF-13-046-APC.

[20] W. Fischer et al., in Proceedings of the 2013 International Particle Accelerator Conference (IPAC13), Shanghai, China, May 2013, p. 1526.

[21] H. Pfeffer and G. Saewert, J. Instrum. **6**, P11003 (2011).

[22] I. Morozov et al., in Proceedings of the 2012 International Particle Accelerator Conference (IPAC12), New Orleans, LA, USA, May 2012, p. 94, FERMILAB-CONF-12-126-APC.

[23] V. Previtali et al., in Proceedings of the 2013 International Particle Accelerator Conference (IPAC13), Shanghai, China, May 2013, p. 993, FERMILAB-CONF-13-154-APC.

[24] V. Previtali et al., FERMILAB-TM-2560-APC (July 2013).

[25] A. Valishev, FERMILAB-TM-2584-APC (May 2014).

[26] G. Stancari et al., in Proceedings of the 52nd ICFA Advanced Beam Dynamics Workshop on High-Intensity and High-Brightness Hadron Beams (HB2012), Beijing, China, September 2012, p. 466, FERMILAB-CONF-12-506-AD-APC.

[27] G. Stancari et al., in Proceedings of the ICFA Workshop on Beam-Beam Effects in Hadron Colliders (BB2013), Geneva, Switzerland, March 2013, FERMILAB-CONF-13-054-APC.

[28] G. Valentino et al., Phys. Rev. ST Accel. Beams **16**, 021003 (2013).

[29] J.-L. Vay et al., Comput. Sci. Disc. **5**, 014019 (2012).

[30] G. Stancari et al., in Proceedings of the 2013 North American Particle Accelerator Conference (NAPAC13), Pasadena, California, 29 September – 4 October 2013, paper ID TUPAC15, FERMILAB-CONF-13-356-APC.

[31] G. Stancari, FERMILAB-FN-0972-APC, arXiv:1403.6370 [physics.acc-ph] (March 2014).

[32] A. Burov et al., Phys. Rev. E **59**, 3605 (1999).

[33] A. Sharapa et al., Nucl. Instrum. Methods Phys. Research A, **406**, 169 (1998).

[34] A. Ivanov and M. Tiunov, in Proceedings of the 2002 European Particle Accelerator Conference (EPAC02), Paris, France, June 2002, p. 1634.

[35] S. Li and G. Stancari, FERMILAB-TM-2542-APC (August 2012).

[36] V. Moens, Masters Thesis, École Polytechnique Fédérale de Lausanne (EPFL), Switzerland, FERMILAB-MASTERS-2013-02 and CERN-THESIS-2013-126 (August 2013).

[37] H. Schmickler, 'Possible alternatives for halo scraping at the LHC,' talk presented at the Special Collimation Upgrade Specification Meeting: Internal Review of Tevatron Hollow Electron-Lens Usage at CERN, https://indico.cern.ch/event/213752, Geneva, Switzerland, 9 November 2012.

[38] S. Maury et al., in Proceedings of the 2013 International Particle Accelerator Conference (IPAC13), Shanghai, China, May 2013, p. 2651.

[39] S. Holmes et al., Run II Handbook, FERMILAB-TM-2484 (1998).

[40] O. Brüning et al., LHC Design Report, CERN-2004-003-V-1 (2004).

[41] V. Scarpine et al., in Proceedings of the 2006 Beam Instrumentation Workshop, Batavia, Illinois, USA, May 2006, FERMILAB-CONF-06-140-AD, AIP Conf. Proc. **868**, 481 (2006).

[42] B. Salvant, private communication (November 2012).

[43] O. Brüning and F. Willeke, in Proceedings of the 4th European Particle Accelerator Conference (EPAC94), London, United Kingdom, June 1994, p. 991.

[44] O. Brüning and F. Willeke, Phys. Rev. Lett. **76**, 3719 (1996).

[45] W. Hofle, private communication (2012).